Journal of Biomedical Optics

BiomedicalOptics.SPIEDigitalLibrary.org

Performance analysis of optical coherence tomography in the context of a thickness estimation task

Jinxin Huang
Jianing Yao
Nick Cirucci
Trevor Ivanov
Jannick P. Rolland

SPIE.

Performance analysis of optical coherence tomography in the context of a thickness estimation task

Jinxin Huang,[a,*] Jianing Yao,[b] Nick Cirucci,[b] Trevor Ivanov,[b] and Jannick P. Rolland[b]
[a]University of Rochester, Department of Physics and Astronomy, 206 Bausch and Lomb Hall, Rochester, New York 14627, United States
[b]University of Rochester, The Institute of Optics, 275 Hutchison Road, Rochester, New York 14627, United States

Abstract. Thickness estimation is a common task in optical coherence tomography (OCT). This study discusses and quantifies the intensity noise of three commonly used broadband sources, such as a supercontinuum source, a superluminescent diode (SLD), and a swept source. The performance of the three optical sources was evaluated for a thickness estimation task using both the fast Fourier transform (FFT) and maximum-likelihood (ML) estimators. We find that the source intensity noise has less impact on a thickness estimation task compared to the width of the axial point-spread function (PSF) and the trigger jittering noise of a swept source. Findings further show that the FFT estimator yields biased estimates, which can be as large as 10% of the thickness under test in the worst case. The ML estimator is by construction asymptotically unbiased and displays a 10× improvement in precision for both the supercontinuum and SLD sources. The ML estimator also shows the ability to estimate thickness that is at least 10× thinner compared to the FFT estimator. Finally, findings show that a supercontinuum source combined with the ML estimator enables unbiased nanometer-class thickness estimation with nanometer-scale precision. [DOI: 10.1117/1.JBO.20.12.121306]

Keywords: optical coherence tomography; broadband source noise; uncertainty analysis; thickness estimation.

Paper 150291SSR received May 2, 2015; accepted for publication Aug. 10, 2015; published online Sep. 17, 2015.

1 Introduction

Optical coherence tomography (OCT) has been widely applied in imaging at micron-scale resolution and deep into the samples under investigation. Because of the unique ability of OCT to highly resolve layers in depth, one of the most common and quantitative tasks of interest is thickness estimation. Prior works have reported using OCT for thickness estimation of different biological layers, including nerve fiber layer,[1] macular,[2] cornea,[3] retina,[4] choroidal,[5] epidermal skin,[6] tear film,[7] and airway.[8]

Regardless of the specific estimation task, it is of great importance to understand the measurement uncertainty associated with the optical system noise, such as the noise of the broadband source. Currently, three types of broadband sources are commonly employed in Fourier domain OCT systems, supercontinuum sources, superluminescent diodes (SLDs), and swept sources. Supercontinuum generation employs a high-repetition rate laser and a nonlinear fiber[9] to achieve extreme nonlinear broadening of optical pulses that may expand a wavelength range to as large as 400 to 2500 nm. On the other hand, SLDs utilize the cavity-free continuous-wave amplified spontaneous emission without optical feedback to produce an emission band centered within the range of 400 and 1700 nm with a typical full width at half maximum (FWHM) bandwidth limited to <190 nm. The different natures of the photon generation processes lead to variations in the noise properties of the two sources. Supercontinuum generation has been long regarded as possessing significantly higher relative intensity noise due to pulse-to-pulse fluctuations. For swept sources, the broadband spectra are temporally encoded by the rapid wavelength sweep over a broad wavelength range. In addition to the source intensity noise, a swept source system is inclined to suffer from jittering noise in the A-scan trigger signals that control the synchronization of the data acquisition with the sweep cycles. Swept source OCT systems are widely employed due to their high speed and long range imaging capability at the common spectra bands around the 1300 and 1500 nm regimes.

The noise characterization of broadband sources has been an important topic in the OCT community. An early study was reported to quantify the noise of SLD by analyzing the detector readings with a radio-frequency spectrum analyzer;[10] in a more recent study, image contrast was reported to evaluate the noise of SLD and supercontinuum.[11] This paper quantifies the noise of three types of OCT sources and further investigates the impact of these sources of noise on a thickness estimation task using two different estimators.

In a quantitative imaging task, an observer is present to make a decision based on the image data.[12] For a thickness estimation task, the observer is an estimator that makes the estimate based on the OCT data. The most commonly used estimator performs a fast Fourier transform (FFT) followed by a peak detection technique in order to compute the optical path difference (OPD) between two peaks defining a layer.[13] This estimator will thereafter be referred to as the FFT estimator. The thickness is then

*Address all correspondence to: Jinxin Huang, E-mail: jxhuang@pas.rochester.edu

estimated by dividing the OPD by the group index of refraction of that layer. The axial resolution achieved with the FFT approach is limited by the width (FWHM) of the axial point-spread function (PSF), which is on the order of a micron in the highest definition systems.[14] Biofilms or biolayers in the order of tens of nanometers are typically not resolved using the FFT approach. These layers may include the lipid and aqueous layers of a tear film,[15] for example. To overcome this limitation, we have recently reported a maximum-likelihood (ML) estimator for the tear film thickness measurement.[16–18]

The purpose of this study is to benchmark the noise properties of different broadband sources, including supercontinuum, SLD, and swept sources, and to investigate the performance of different sources for a thickness estimation task, with both FFT and ML estimators. For such a purpose, the rest of the paper is organized as follows. Section 2 presents a Fourier domain OCT mathematical model that provides the foundation for noise quantification and performance discussion; Sec. 3 quantifies the intensity noise of a supercontinuum source, an SLD, and a swept source; Sec. 4 first benchmarks the performance of different sources using both the FFT and ML estimators in a general one-layer thickness estimation task through simulation; we then experimentally validate the key simulation findings before we conclude.

2 Fourier Domain Optical Coherence Tomography Modeling

The formulation of a mathematical description of a spectral domain OCT system was first reported in our prior work.[17,18] Since a swept source system is also discussed in this paper, we emphasize the key points of the mathematical constructs here and generalize the model to describe a more general Fourier domain OCT, as they closely pertain to the noise characterization and the estimators we employed for the thickness estimation task. Figure 1 shows a schematic of the system based on a Michelson interferometer configuration. The broadband light source emits an electric field denoted as $E_s(\omega, t)$, where ω is the angular frequency. It is split at the beam splitter and propagates to both reference and sample arms. The response $m_r(\omega)$ associated with the electric field $E_s(\omega, t)$ following its propagation through the reference arm can be written as

$$m_r(\omega) = \frac{1}{2} r \cdot \exp\left(i2n_0 \frac{\omega}{c} l_r \right), \tag{1}$$

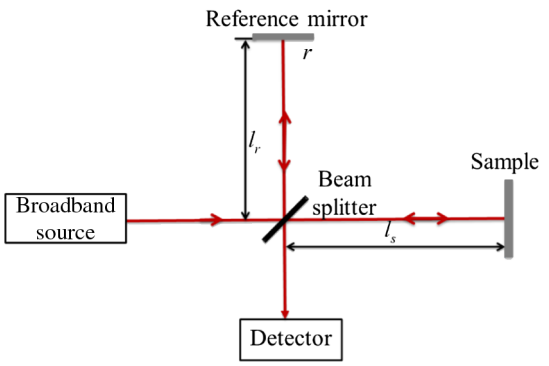

Fig. 1 Schematic layout of a Fourier domain optical coherence tomography (OCT) setup.

where r is the reflectance of the mirror, n_0 is the refractive index of air, c is the velocity of light in vacuum, and l_r is the length of the reference arm. This term is set to be zero when a common path configuration is used. Similarly, the response from the sample arm is denoted as $m_s(\omega)$, which depends on the specific sample.

The backreflected/scattered light from both arms recombines at the beam splitter, and the resulting interference pattern is collected by the detector. For a spectral domain OCT, the detector is a spectrometer in which a dispersive element is used to disperse the light. A high-speed line-scan camera, with tens of thousands of A-scans per second, records the intensity of the modulated signal and maps the wavelength information to the indices of different camera pixels. For the case of a swept source OCT, the detector is a photodiode in which the wavelength information is encoded by time stamps. For either a spectrometer-based OCT or a swept source OCT, the output of one A-scan is a discretized spectrum $\mathbf{N_g}$, which is an array with M elements, where M is the number of pixels or time stamps. $N_g(\lambda_i, \Delta t)$ is proportional to the number of electrons accumulated in the narrow band centered at λ_i during the detector integration time Δt. Given the laser intensity noise as well as the Poisson noise and dark noise of the detector, the randomness of $N_g(\lambda_i, \Delta t)$ may be approximated by a normal distribution as in Ref. 16

$$N_g(\lambda_i, \Delta t) \sim \text{Normal}(\langle\langle\langle N_g(\lambda_i, \Delta t)\rangle\rangle\rangle, K_{N_g}(\lambda_i, \Delta t)), \tag{2}$$

in which $\langle\langle\langle N_g(\lambda_i, \Delta t)\rangle\rangle\rangle$ represents the ensemble's average of the output over laser intensity noise, Poisson noise, and dark noise. $K_{N_g}(\lambda_i, \Delta t)$ denotes the variance of the readout and is given as in Ref. 16

$$K_{N_g}(\lambda_i, \Delta t) = C_1 \langle\langle\langle N_g(\lambda_i, \Delta t)\rangle\rangle\rangle^2 + C_2 \langle\langle\langle N_g(\lambda_i, \Delta t)\rangle\rangle\rangle + C_3, \tag{3}$$

where the coefficients C_1, C_2, and C_3 correspond to the laser intensity noise, Poisson noise, and dark noise, respectively. The values of the coefficients are quantified for three different broadband sources in the following section.

3 Noise Measurements of Different Broadband Sources

To benchmark the intensity noise levels of different sources, a supercontinuum source (WhiteLase Micro, Fianium), an SLD (Broadlighter D840, Superlum), and a swept source (Santec, HSL-2100-WR) have been studied. To measure the source intensity noise, only the reference arm is used. A variable neutral density filter (VNDF), which was placed before the input of the detector in order to avoid stray light or any potential light leakage, was used to adjust the level of light incidence on the detector in the context of noise measurements as a function of the overall light power. Readings from one chosen pixel or time stamp were recorded for a fixed light intensity level, from which the mean and variance of the digital number were calculated. Then as we adjusted the position of the VNDF, the intensity of the light reaching the detector monotonically increased. After quantifying the mean and the corresponding variance at different light intensity levels, the relation of the variance of the power spectrum $K_{N_g}(\lambda_i, \Delta t)$ versus its mean value $\langle\langle\langle N_g(\lambda_i, \Delta t)\rangle\rangle\rangle$ is plotted in Fig. 2, for a supercontinuum, a swept source, and an SLD, respectively. The coefficients C_1, C_2, C_3 of the curves were evaluated for each source and are listed in Table 1. The

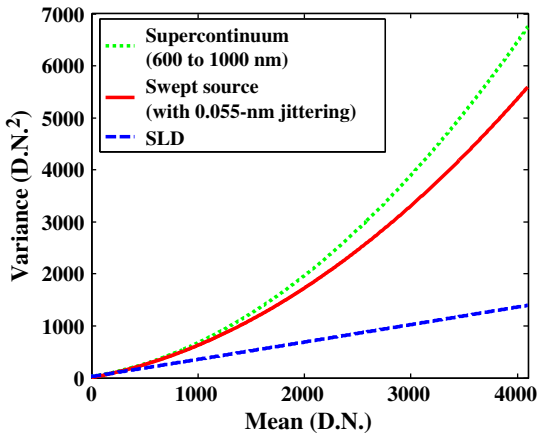

Fig. 2 Relation between the output variance of the power spectrum and the mean value (D.N.: digital number) for three different broadband sources.

Table 1 Second-order polynomial fitting coefficients of optical coherence tomography (OCT) system noise for different sources.

Source type	C_1	C_2	C_3
Supercontinuum Fianium WhiteLase Micro	3.2×10^{-4}	0.33	25
SLD Superlum Broadlighter D840	1.1×10^{-6}	0.33	25
Swept source Santec HSL-2100-WR	2.4×10^{-4}	0.38	6

results show that the SLD has the least intensity noise, followed by the swept source, and then the supercontinuum. It is important to note that, besides the intensity noise, the swept source may suffer from trigger jittering, which may impose an uncertainty in the wavelength, and thus affect its performance in thickness estimation. The following section discusses the swept source in two cases: (1) in the best scenario, an ideal swept source is considered with only intensity noise and (2) a swept source, in a real lab setting, is investigated with trigger jittering noise.

4 Investigation of Source Performance with Different Estimators

This section investigates the performance of three optical sources for a thickness estimation task. We first discuss how to generate simulated spectra in Sec. 4.1. Then in Secs. 4.2 and 4.3, the performances of the three optical sources are investigated through simulations for the FFT and ML estimators, respectively, using the accuracy and precision of thickness estimates as system performance metrics. Experimental measurements are performed in Sec. 4.4 to validate the key findings in Secs. 4.2 and 4.3.

4.1 *Generating Simulated Spectra*

To compare the performance of three sources in simulation, their spectra were first scaled to the same level (i.e., 50%) of the full scale of the detector. To benchmark the performance, a Schott AF 32® Eco thin glass layer that has a known dispersion was used in this study as the sample. In the study, the first surface of the thin glass was used as the reference as a means, in practice, of eliminating the impact of potential vibrations. From Eqs. (2) and (3), a simulated spectrum can be generated from a Gaussian random number generator for the supercontinuum and SLD sources. For the swept source, a random wavelength shift ($\Delta\lambda_i$) with a standard deviation of 0.055 nm was taken into account considering the jittering characteristic of the A-scan trigger signal experimentally measured by an oscilloscope. Mathematically, to generate one simulated spectrum for the swept source, a random wavelength array was first generated using the following equation:

$$\lambda_i \sim \text{Normal}(\bar{\lambda}_i, \Delta\lambda_i^2). \tag{4}$$

With the jittered wavelength array, Eqs. (2) and (3) were then used to generate a simulated spectrum for a swept source.

4.2 *Principle of the Fast Fourier Transform Estimator and Simulations*

In a Fourier domain OCT, the depth information of the sample is encoded in the oscillation modulation frequency of the spectrum. Thus, for each simulated spectrum, an FFT was performed to yield a depth profile that contains the information of the intensity of the backreflected signal along the depth of the sample. An example of a depth profile is shown in Fig. 3, where two major peaks are located at the axial positions representing the optical paths of the layer surfaces. It is noted that zero padding on the interference spectrum was conducted prior to the FFT to ensure that the peaks were sampled at a sampling resolution of 1 nm. The group optical thickness of the layer was then obtained from the difference of the two peak locations. Due to the low-coherence interferometry nature of OCT, the directly measured OPD is a product of the physical thickness and the group refractive index of the layer. The group index (n_g) is associated with the phase index (n_p) based on the dispersion relation $n_g(\lambda_i) = n_p(\lambda_i) - \lambda_i[\partial n_p(\lambda)/\partial\lambda]_{\lambda_i}$, where $[\partial n_p(\lambda)/\partial\lambda]_{\lambda_i}$ is the dispersion

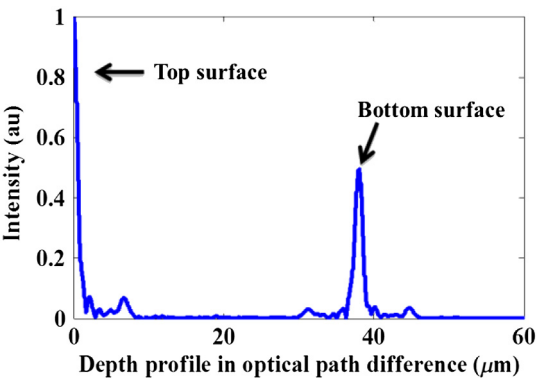

Fig. 3 Depth profile of a spectrum after fast Fourier transform (FFT).

slope at a wavelength λ_i.[19] Therefore, to estimate the physical thickness of the layer, the measured group optical thickness is further divided by the group index estimated at the central frequency of the OCT operating spectral band.

To compare the performance of three sources, the ground truth of the thickness in the simulations was scaled with the width (FWHM) of the axial PSFs of three sources for the glass film under discussion (refractive index of 1.5), which are 0.9, 3.3, and 6.5 μm, for the supercontinuum, SLD, and swept sources, respectively. In the following Secs. 4.2.1 to 4.2.3, the thickness estimation task is performed in three thickness ranges: the thickness to be measured is (1) larger than 10 times the width of the axial PSFs, (2) between 1 to 10 times the width of the axial PSFs, and (3) less than the width of the axial PSFs.

4.2.1 *Thickness 10 times larger than the width of axial point-spread functions*

In this section, simulations were set up for estimating layer thicknesses with ground truth ranging from 10 to 100 times the width of axial PSFs for all three sources. Figure 4 shows the deviation of the estimated mean thickness from the ground truth as well as the standard deviation of the measurements obtained from repeated estimates on a set of 2000 simulated spectra. Results show that estimates from all three sources are slightly biased compared to the ground-truth thickness. The standard deviations of the estimates for the supercontinuum, SLD, and swept sources without wavelength jittering are within 2, 6, and 8 nm, respectively. It is worth noting that when only source intensity noise is present, all three sources have a precision as good as a few nanometers. The fact that the supercontinuum source has the most precise estimates can be explained by the fact that it has the finest axial PSF. When the trigger jittering noise is considered, the estimation precision of the swept source gets significantly worse as the ground-truth thickness increases. For a thickness ground truth of 100 times that of the swept source axial PSF, the jittering noise causes the estimation precision to increase by a factor of 8. By comparing the performance across the three different sources, results show that the source intensity noise has less impact on a thickness estimation task compared to the impact of the axial PSF or the trigger jittering noise.

The presence of biased estimates in all three sources may be explained by the following observations: (1) the dispersion property of the sample sets the apparent group index that may not be accurate to describe the propagation of a broadband light in the sample. Dividing the group optical thickness by a fixed group index computed at the central frequency of OCT may result in an inaccurate thickness estimation and (2) zero padding of the spectrum is used to achieve a finer sampling step (i.e., 1 nm) in the depth profile, which is equivalent to performing a sinc interpolation to the depth profile.[20] The sinc interpolation is an approximation of the location of the axial depth peaks.

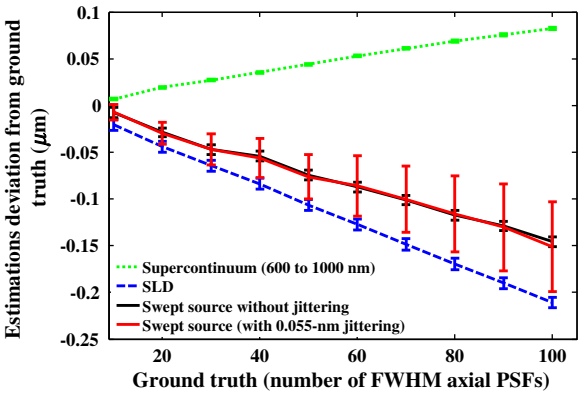

Fig. 4 Estimates bias and precision for the FFT estimator.

4.2.2 *Thickness in the same order of magnitude as the width of axial point-spread functions*

In this section, the thickness of the ground truth under discussion ranges from 1 to 10 times the width of the axial PSFs. The rest of the parameters in the simulations were the same as in Sec. 4.2.1. The bias and precision of the estimates are shown in Figs. 5 and 6, respectively. The supercontinuum, SLD, and swept sources without trigger jittering have comparable precision as they have in the previous section; for a swept source with jittering noise, the precision was better than that shown in Sec. 4.2.1, where a larger thickness was presented. The different behaviors of the swept source show that trigger jittering noise has less impact on thinner thickness estimates, where the spectrum has less dense oscillations. On the other hand, for thinner estimates, biases of as much as 10% of the absolute thickness under test are observed when the ground truth is less than twice of the axial PSFs for all three sources. The bias fluctuates as the ground-truth thickness changes; the amplitude of the fluctuation gradually gets smaller and flattens when the ground-truth thickness is larger than eight times the axial PSFs.

Compared to the previous task where the thickness was >10 times the width of the axial PSFs, here the ground truth is between 1 and 10 times the width of the axial PSFs. Results yield a larger bias, which means the thickness estimation task becomes more challenging for the FFT estimator when the thickness under test is closer to the width of the axial PSFs. The difficulty in estimating thicknesses closer to the width of the axial PSFs may be explained by the fact that the two peaks in the depth profile, which correspond to the two surfaces of a layer, start to have more of an impact on each other. For example, sidelobes of the first peak can cause a shift of the second peak location and, thus an associated biased thickness estimate.

4.2.3 *Thickness less than the width of the axial point-spread functions*

As shown in Sec. 4.2.2, the task has become more challenging for the FFT estimator when the ground-truth thickness is comparable to the width of the axial PSFs. When the thickness under test is even thinner than the width of the axial PSFs, the FFT estimator is expected to breakdown. In Fig. 7(a), the performance of the FFT estimator is simulated for a Schott AF 32® Eco layer ranging from 0.1 to 4.9 μm thick in 0.2 μm intervals for the supercontinuum source. As expected, the FFT estimator breaks down by a significant bias error in the case where the layer thickness is smaller than the width of the axial PSF. Figure 7(b) shows the depth profile of a film with a 0.1-μm thickness after Fourier transform of the simulated spectrum. It can be seen that the two peaks representing the top and bottom surfaces of the layer are unresolvable due to the optical thickness of the sample falling well below the width of the axial PSF of the OCT system. The FFT estimator mistakenly detects a side lobe

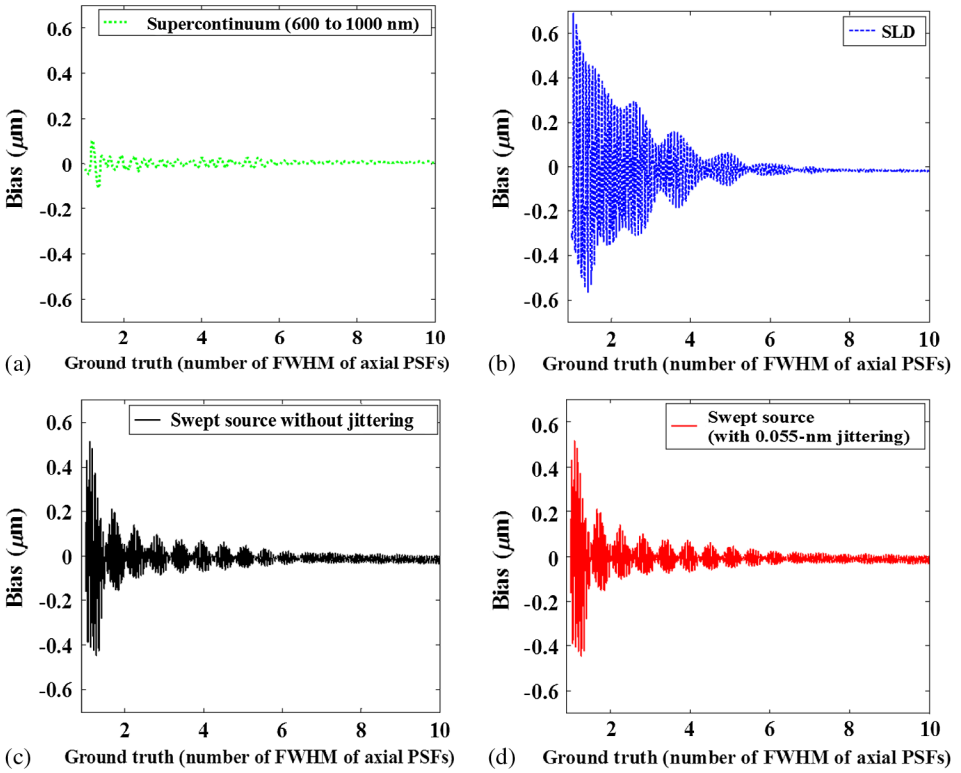

Fig. 5 Estimation bias for the FFT estimator with optical sources of (a) a supercontinuum, (b) a superluminescent diode (SLD), (c) a swept source without jittering, and (d) a swept source with jittering.

as the peak representing the bottom surface and as such a large biased result.

4.3 *Principle of the Maximum-Likelihood Estimator and Simulations*

This section benchmarks the performance of the ML estimator. In a Fourier domain OCT system, the final output from the system is a spectrum $\mathbf{N_g}$. From the ML estimation framework, the probability of observing one simulated spectrum $\mathbf{N_g}$ from a possible thickness d can be expressed as in Ref. 18

$$P(\mathbf{N_g}|d) = \frac{1}{(2\pi)^{\frac{M}{2}}\prod_i [K_{N_g}(\lambda_i, \Delta t)]^{\frac{1}{2}}} \exp \times \left\{ -\frac{1}{2}\sum_i \frac{[N_g(\lambda_i, \Delta t) - \langle\langle\langle N_g(\lambda_i, \Delta t)\rangle\rangle\rangle]^2}{K_{N_g}(\lambda_i, \Delta t)} \right\}, \tag{5}$$

where M is the number of pixels or time stamps, $N_g(\lambda_i, \Delta t)$ is the intensity of the one spectrum at the wavelength λ_i, and $\langle\langle\langle N_g(\lambda_i, \Delta t)\rangle\rangle\rangle$ and $K_{N_g}(\lambda_i, \Delta t)$ represent the mean and variance of the spectrum that is associated with a possible thickness d at wavelength λ_i. The ML method estimates the thickness by maximizing $P(\mathbf{N_g}|d)$, which yields

$$\hat{d} = \underset{d}{\operatorname{argmin}}\{-\log[P(\mathbf{N_g}|d)]\}. \tag{6}$$

To compare with the FFT estimator, we benchmarked the performance of the ML estimator based on evaluating the same set of spectra simulated for a Schott AF 32® Eco thin glass film. A thickness ranging from 0.1 to 1 time the width of axial PSFs is also discussed, in addition to thicknesses that are larger than the width of the axial PSFs. The estimated mean and precision obtained from the ML estimator for all three sources are shown in Figs. 8(a) and 8(b). Results show that the ML estimator is unbiased for all three sources across the whole thickness ranging from 0.1 to 100 times the width of axial PSFs. For the thickness range that is less than the width of the axial PSFs, all sources yield a precision better than 5 nm. With a thickness larger than the width of the PSFs, both supercontinuum and SLD yield a precision better than 0.3 nm. However, for the swept source

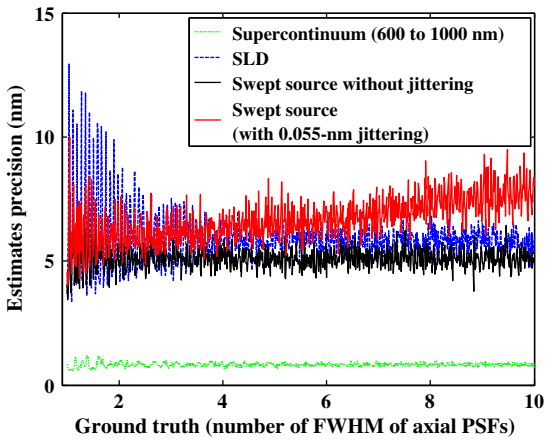

Fig. 6 Estimation precision for the FFT estimator with optical sources of a supercontinuum, an SLD, a swept source without jittering, and a swept source with jittering.

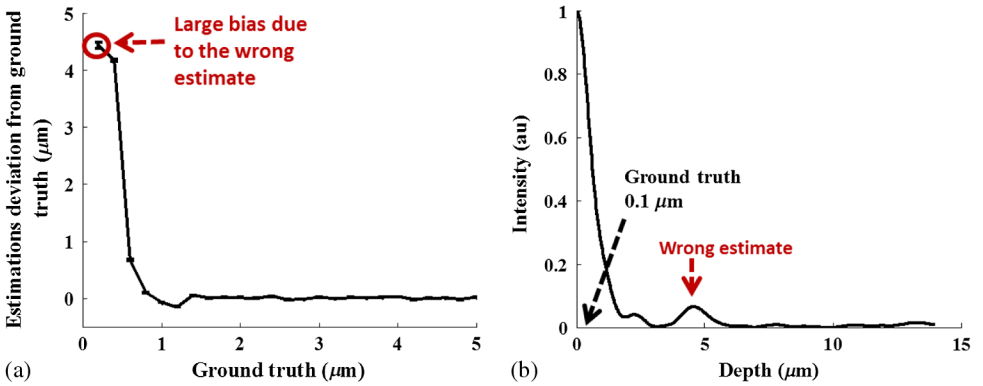

Fig. 7 (a) The breakdown of FFT estimator for thicknesses less than the width of the axial point-spread function (PSF) and (b) the illustration of the FFT picks the wrong peak for the estimate.

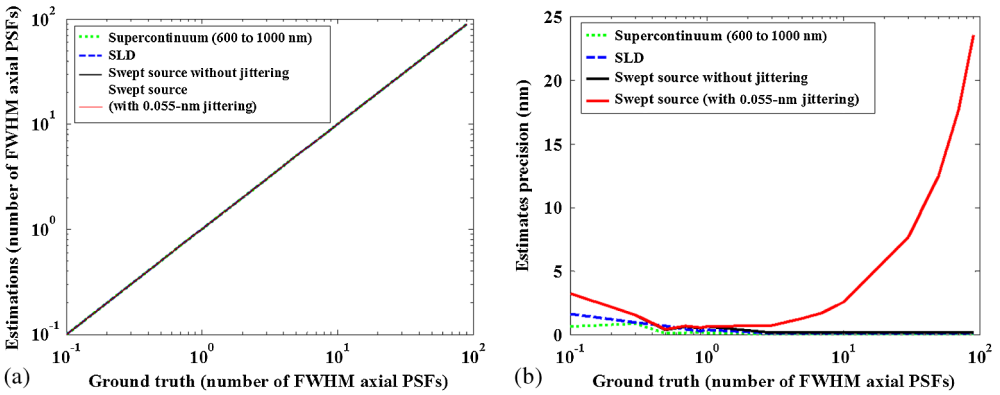

Fig. 8 Simulation results for the maximum-likelihood (ML) estimator: (a) the mean estimations versus the ground truth and (b) estimation precisions for different sources.

with jittering noise, the precision gets worse when the ground-truth thickness increases. Compared to the FFT estimator, the precisions of the supercontinuum and SLD sources are improved by an order of magnitude; however, for the swept source with jittering noise, the precision is improved by only a factor of 2, which is due to the fact that the ML estimator does not have the priori knowledge of the wavelength shift.

4.4 *Experimental Validation*

In Secs. 4.2 and 4.3, results show that the FFT estimator yields biased estimates, while the ML estimator is, by construction, asymptotically unbiased and is shown to be more immune to the source intensity noise, displaying a 10× improvement in precision for the supercontinuum and SLD sources. To further validate these findings, the supercontinuum source, which offers the best performance in simulation, is chosen to carry out the experiments that will be discussed in the following sections.

4.4.1 *Customized optical coherence tomography instrumentation*

A custom free-space spectral-domain ultrabroadband OCT system, as shown in Fig. 9, was used for the experimental validation. The system layout was detailed in our previous study.[16] In summary, the key components of the system consist of a commercial broadband light source, a custom bandpass filter, and a custom broadband astigmatism-corrected Czerny–Turner spectrometer.[21] The supercontinuum laser (WhiteLase Micro, Fianium) is filtered to operate in the spectral window of 600 to 1000 nm. The light, after passing the custom filter, is split into the reference and sample arms by a 50/50 nonpolarizing cube beamsplitter (BS014, Thorlabs Inc.). In the sample arm, a galvanometer-based scanner (Dual axis, Cambridge Technologies Inc.) coupled with a broadband near-infrared achromatic focusing objective (EFL = 40 mm, Thorlabs Inc.) directs the beam to the sample for telecentric scanning. The beam size is 2 mm in diameter ($1/e^2$ of the maximum), yielding a 20-μm FWHM lateral PSF. In the reference arm, an equivalent lens is used for dispersion compensation. The back reflection/scattering light beams from both arms are focused into a broadband astigmatism-corrected Czerny–Turner spectrometer. The spectrometer interfaces to a line-scan camera of 8192 pixels (SPL8192-70 km, Basler Inc.) that yields a 0.1-nm spectral resolution. The integration time of the camera was set at 20 μs in all follow-up measurements.

4.4.2 *Measurement of a glass film*

To validate the simulation results, a Schott AF 32® Eco glass film in the laboratory was used as the sample. A 50-μW power incidence was chosen for the purpose of the glass film measurement because it displays high reflectivity; the sensitivity was measured to be 88 dB. For other applications, such as eye imaging, the power incidence on the sample is adjusted to be 0.7 mW, which is much higher yet complies with the American National Standards Institute standards, and, in this case, the sensitivity was measured to be 108 dB. In the experiment,

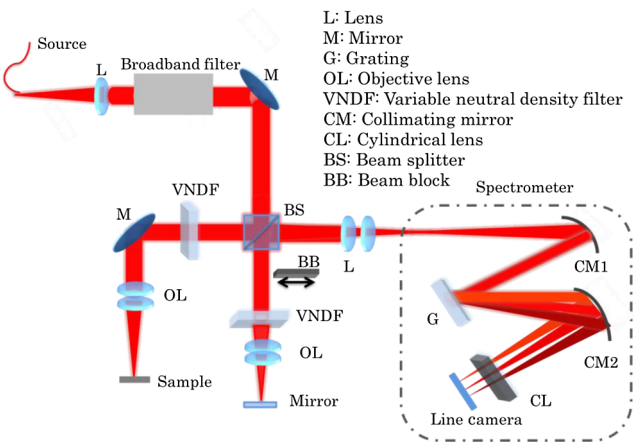

Fig. 9 Custom spectral-domain OCT experimental setup.

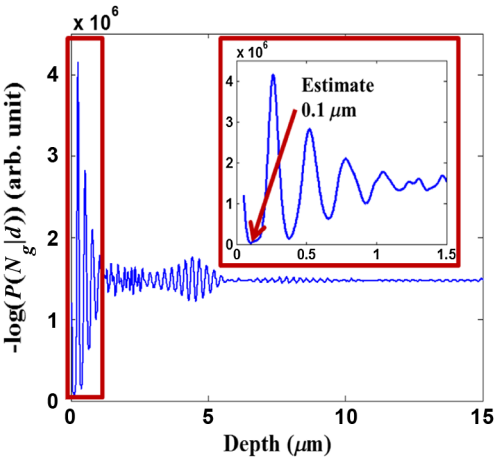

Fig. 10 The probability distribution calculated by the ML estimator for a spectrum from a 0.1-μm layer.

we acquired 5000 spectra from the glass film under test. The spectra were then processed using both the FFT and ML approaches. Results yield 26.841 ± 0.004 and 26.8201 ± 0.0003 μm for the FFT and the ML estimators, respectively. It is noteworthy that the mean thickness measured by the FFT approach has a 21-nm discrepancy compared to that of the ML estimator, which agrees with the prediction from the simulations shown in Fig. 4. The precision of the ML estimator is also validated to be 10× better than that of the FFT estimator.

4.4.3 *Performance of the maximum-likelihood estimator for extremely thin layers*

Results in Fig. 8(a) show that the ML estimator can estimate a thin thickness, at least down to one-tenth the width of the axial PSFs. To demonstrate the capability of the ML estimator in measuring thicknesses significantly less than the width of the axial PSFs, a phantom was fabricated by depositing a Ta_2O_5 coating on a LaSFn9 glass substrate. The thickness ground truth of the phantom was made to be 99.0 ± 2.0 nm.

To experimentally validate the performance of the ML estimator for measuring such a small thickness, 2000 spectra were acquired from the center of the phantom and were processed by the ML estimator. The measured average thickness was found to be 99.5 ± 0.5 nm, which was within the thickness range of the

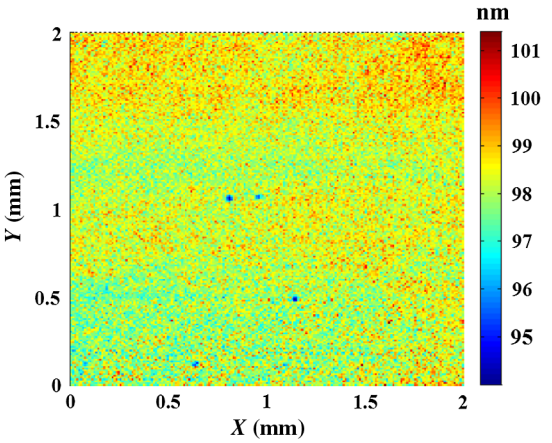

Fig. 11 Thickness map of a physical phantom.

ground truth. An example of a probability distribution plot used by the ML estimator to predict a thickness of 0.1 μm is shown in Fig. 10.

After validation at one single point, a telecentric scanning of a 2 mm × 2 mm on the phantom was taken, with 200 × 200 points that corresponds to a 10-μm sampling resolution. The thickness map is shown in Fig. 11, in which the mean thickness over the 2 mm × 2 mm area was calculated to be 98.3 nm with a 0.6-nm surface root-mean-square error.

5 Conclusion

This study benchmarked the noise levels of three of the most commonly used broadband sources in Fourier domain OCT, i.e., a supercontinuum, an SLD, and a swept source. Results show that the SLD has the least intensity noise, followed by the swept source, and the supercontinuum. From the quantified noise, we studied the performance of these three sources in the context of a thickness estimation task using both FFT and ML estimators. Findings show that source intensity noise has less impact on a thickness estimation task compared to the axial PSF and trigger jittering of a swept source.

The FFT estimator has slightly biased estimates when the thickness under test is more than 10 times the width of the axial PSFs, and the precision can be as good as several nanometers. However, when the thickness to be estimated is on the same order of magnitude as the width of the axial PSF, the thickness estimation becomes challenging for the FFT estimator as it yields a large bias that may reach as much as 10% of the thickness under test. As the thickness to estimate becomes even thinner than the width of the axial PSF, the FFT estimator breaks down and cannot provide meaningful estimates. With the ML estimator, all sources yield unbiased estimates, with the capability to estimate thinner thicknesses down to at least one-tenth of the width of the axial PSF. For both the supercontinuum and SLD, the estimates can be achieved with a precision that is an order of magnitude better compared to the FFT estimator. In the case of the swept source, because it typically suffers from trigger jittering noise, the precision of the estimates is improved compared to the FFT estimator by only a factor of 2.

Finally, this paper quantifies the various amount of noise in a supercontinuum, an SLD, and a swept source, accounting for jitter noise in the case of the later. Results show that while the supercontinuum is noisiest among the three sources considered, it, in fact, yields the most precise estimates with nanometer-scale precision and is able to achieve unbiased estimates for tens of

nanometer thicknesses when combined with the ML estimator. This finding can be attributed to the fact that intensity noise in the source is only one component to consider in performing an estimation task and that the ability to create a broad spectrum such as >200 nm at the central wavelength of 800 nm is a critical component of the task.

Acknowledgments

We acknowledge Eric Clarkson and Matthew Kupinski for stimulating discussion on mathematical observers upon which this paper on metrology builds. We thank the II-VI Foundation for supporting this research on metrology with OCT. This research benefitted from NSF REU supplements to the NSF I/UCRC Center for Freeform Optics (IIP-1338877) and the NSF grant (No. EECS-1002179).

References

1. J. S. Schuman et al., "Reproducibility of nerve fiber layer thickness measurements using optical coherence tomography," *Ophthalmology* **103**(11), 1889–1898 (1996).
2. D. S. Greenfield, H. Bagga, and R. W. Knighton, "Macular thickness changes in glaucomatous optic neuropathy detected using optical coherence tomography," *Arch. Ophthalmol.* **121**(1), 41–46 (2003).
3. S. Muscat et al., "Repeatability and reproducibility of corneal thickness measurements by optical coherence tomography," *Invest. Ophthalmol. Vis. Sci.* **43**(6), 1791–1795 (2002).
4. H. Sánchez-Tocino et al., "Retinal thickness study with optical coherence tomography in patients with diabetes," *Invest. Ophthalmol. Vis. Sci.* **43**(5), 1588–1594 (2002).
5. V. Manjunath et al., "Choroidal thickness in normal eyes measured using Cirrus HD optical coherence tomography," *Am. J. Ophthalmol.* **150**(3), 325–329 (2010).
6. T. Gambichler et al., "In vivo data of epidermal thickness evaluated by optical coherence tomography: effects of age, gender, skin type, and anatomic site," *J. Dermatol. Sci.* **44**(3), 145–152 (2006).
7. J. Wang et al., "Precorneal and pre-and postlens tear film thickness measured indirectly with optical coherence tomography," *Invest. Ophthalmol. Vis. Sci.* **44**(6), 2524–2528 (2003).
8. H. O. Coxson et al., "Airway wall thickness assessed using computed tomography and optical coherence tomography," *Am. J. Resp. Crit. Care* **177**(11), 1201–1206 (2008).
9. J. M. Dudley, G. Genty, and S. Coen, "Supercontinuum generation in photonic crystal fiber," *Rev. Mod. Phys.* **78**(4), 1135–1184 (2006).
10. S. Shin et al., "Characterization and analysis of relative intensity noise in broadband optical sources for optical coherence tomography," *IEEE Photon. Technol. Lett.* **22**(14), 1057–1059 (2010).
11. W. J. Brown, S. Kim, and A. Wax, "Noise characterization of supercontinuum sources for low-coherence interferometry applications," *J. Opt. Soc. Am. A* **31**(12), 2703–2710 (2014).
12. H. H. Barrett and K. J. Myers, *Foundations of Image Science*, Wiley, Hoboken, New Jersey (2004).
13. M. Shahidi, Z. Wang, and R. Zelkha, "Quantitative thickness measurement of retinal layers imaged by optical coherence tomography," *Am. J. Ophthalmol.* **139**(6), 1056–1061 (2005).
14. W. Drexler et al., "Ultrahigh-resolution ophthalmic optical coherence tomography," *Nat. Med.* **7**(4), 502–507 (2001).
15. P. E. King-Smith et al., "The thickness of the tear film," *Curr. Eye Res.* **29**(4–5), 357–368 (2004).
16. J. Huang et al., "Measurement of a multi-layered tear film phantom using optical coherence tomography and statistical decision theory," *Biomed. Opt. Express* **5**(12), 4374–4386 (2014).
17. J. Huang et al., "Maximum-likelihood estimation in optical coherence tomography in the context of the tear film dynamics," *Biomed. Opt. Express* **4**(10), 1806–1816 (2013).
18. J. Huang et al., "Phantom study of tear film dynamics with optical coherence tomography and maximum-likelihood estimation," *Opt. Lett.* **38**(10), 1721–1723 (2013).
19. M. Born and E. Wolf, Eds., *Principles of Optics: Electromagnetic Theory of Propagation, Interference and Diffraction of Light*, 7th ed., Cambridge University Press (1999).
20. L. P. Yaroslavsky, "Efficient algorithm for discrete sinc interpolation," *Appl. Opt.* **36**(2), 460–463 (1997).
21. K. Lee, K. Thompson, and J. P. Rolland, "Broadband astigmatism-corrected Czerny–Turner spectrometer," *Opt. Express* **18**(22), 23378–23384 (2010).

Jinxin Huang is a PhD candidate in the Department of Physics and Astronomy, University of Rochester. He received his BS degree in optical information science and technology from Harbin Institute of Technology, China, in 2009. His research interest includes task-based image quality assessment in the context of optical coherence tomography, with a special emphasis on tear film imaging.

Jianing Yao is a PhD candidate at the Institute of Optics, University of Rochester. She received her BS degree in electronic science and technology from Tianjin University, China, in 2009. Her research interests include the development of methodology and instrumentation for optical coherence tomography (OCT) metrology of freeform optics, including gradient refractive index optical components.

Nick Cirucci received his BS degree in optical engineering at the Institute of Optics, University of Rochester, in spring 2015.

Trevor Ivanov received his BS degree in optical engineering at the Institute of Optics, University of Rochester, in spring 2015.

Jannick P. Rolland is the Brian J. Thompson professor of optical engineering at the Institute of Optics at the University of Rochester. She directs the NSF-I/UCRC Center for Freeform Optics (CeFO), the R.E. Hopkins Center for Optical Design and Engineering, and the ODALab. She is a fellow of OSA and SPIE. She was awarded the 2014 OSA David Richardson Medal for her innovative and advanced contributions to optical engineering, including advancing optical biopsy.